

Decomposition of Dolomite Monitored by Neutron Thermodiffractometry

Antonio H. De Aza, Miguel Angel Rodríguez, José Luis Rodríguez, Salvador De Aza,* and Pilar Pena

Instituto de Cerámica y Vidrio, C.S.I.C., 28500 Arganda del Rey, Madrid, Spain

Pierre Convert and Thomas Hansen

Institut Laue Langevin, 38042 Grenoble, France

Xavier Turrillas

Instituto de Ciencias de la Construcción Eduardo Torroja, C.S.I.C., C/ Serrano Galvache s/n., 28032 Madrid, Spain

Dolomite powder from Coín (Spain) was heated in air at a constant rate of 2°C/min to 1000°C, while neutron diffraction patterns were collected every 150 s. Rietveld refinement was applied and raw intensity data were used to monitor decomposition. The full process happened in two stages: dolomite decomposition to give calcite and periclase, and calcite breakup. The first stage activation energy was 47 kcal·mol⁻¹ from fitting to a contracting sphere model. The dolomite mean thermal expansion coefficients were $(6.7 \pm 0.4) \times 10^{-6}$ and $(2.7 \pm 0.2) \times 10^{-5} \text{ K}^{-1}$ along the *a* and *c* axes, respectively. Changes in the Ca–O and Mg–O bond distances were also measured.

I. Introduction

DOLOMITE, ideal formula $\text{MgCa}(\text{CO}_3)_2$, is a very common mineral in nature. Along with two other calcium carbonates (calcite and aragonite) it makes up ~2% of the earth's crust. Dolomite is a very important industrial mineral.¹ Primarily it is used as a source of both magnesium metal and magnesia. One of the major applications of dolomite is in the field of refractory materials such as sintered dolomite. Dolomite is often used as an aggregate instead of calcite (CaCO_3) in concrete preparation and in the iron and steel industry as a flux. Indeed, it substitutes calcite with advantage as a flux-stone because it is lighter and, from a chemical point of view, more stable, since it does not slake as easily as calcite-based slags do in the presence of water.¹ More recently dolomite has been used in the industrial synthesis of (a) magnesium spinel containing calcium aluminate cements,^{2,3} (b) periclase–calcium zirconate based materials by reaction sintering with zircon,⁴ and (c) reactive coatings on alumina substrates.⁵

All of those applications imply the decomposition of dolomite, hence the necessity and interest of revisiting its decomposition and the topics connected to it, such as stability as a function of temperature, and reaction kinetics.

According to Wyckoff⁶ its crystal structure, although related to calcite, shows distinctive traits. The structure is less symmetrical than calcite, with the cations segregated in different layers, and can

be viewed as a series of alternating layers of CaO_6 octahedra and MgO_6 octahedra separated by CO_3 triangles with the carbon atoms slightly above the three-oxygen plane, while the calcium and magnesium ions are segregated in different layers. It can exhibit some complex order–disorder features at high temperatures. Some calcium layers can contain magnesium cations and conversely some magnesium layers may contain calcium cations. Furthermore, the ratio Ca/Mg can be different from the stoichiometric value. For a comprehensive discussion on this matter see the monograph by Chang, Howie, and Zussman⁷ and also the work of Goldsmith and Heard.⁸

Haul and Heystek⁹ conducted extensive studies on the decomposition of dolomite by differential thermal analysis (DTA), X-ray diffraction, and carbon isotope (¹³C) techniques. They obtained DTA curves under different CO_2 pressures and concluded that in the CO_2 pressure range from 100 to 760 mmHg, dolomite decomposes in two steps. Otsuka¹⁰ summarizes the results, stating that the first step takes place at 775°C to yield calcite and periclase (MgO) accompanied by a release of CO_2 , and the second at 870°C due to the decomposition of calcite. When the CO_2 partial pressure decreases, the 775°C endotherm is shifted to higher temperatures and the 870°C endotherm moves in the opposite direction until the two endotherms merge at pressures <260 mmHg and the decomposition of dolomite proceeds in a single step to yield CaO, MgO, and CO_2 .

A recent paper by Martínez *et al.*¹¹ reports work conducted *in situ* using synchrotron radiation diffraction analysis of dolomite specimens at high pressure and there is another study using conventional X-ray diffraction at high temperature by Engler *et al.*¹² However, the decomposition has never been examined using time-resolved neutron diffraction methods. In principle, the use of powder neutron diffraction (PND) allows data collection at an adequate rate to get an acceptable time resolution. However, a multidetector system and a high neutron flux are then required. Information can hence be collected during the course of the decomposition reaction, and short-lived species could be spotted which otherwise might escape detection. Another important advantage of using neutrons is the ready penetration of thick samples. The experimental data so collected from a reaction taking place in a bulky sample are truly representative since the diffraction signal comes from the whole specimen and not from the rear surface layer.

In the present paper, the results obtained using time-resolved neutron diffraction methods for the *in situ* decomposition of dolomite and its kinetics are discussed. Rietveld refinement has been used to determine lattice constants, atomic positions, and bond distances as a function of temperature. The mean (linear)

R. L. Snyder—contributing editor

Manuscript No. 187931. Received February 16, 2001; approved January 31, 2002. This work was supported by CICYT under Grant No. MAT 2000-0941. Additional support for J. L. Rodríguez was provided through Fellowship CONACYT No. 69147. *Member, American Ceramic Society.

thermal expansion coefficients for the lattice constants and bond distances in dolomite have been also deduced.

II. Experimental Procedure

(1) Chemical Analysis

The specimen used in this study was a natural polycrystalline dolomite powder from the quarries in Coín (Spain) commercialized by Prodomasa (Málaga, Spain) under the name of Micro 15[®]. The composition of this dolomite is very close to the formula $\text{CaMg}(\text{CO}_3)_2$. Its chemical analysis is shown in Table I.

To analyze the chemical composition of the cations, other than calcium and magnesium, the specimen was dissolved in dilute hydrochloric acid and then, depending on the elements sought, different analytical techniques were used as stated in Table I.

(2) X-ray Diffraction

The cell parameters of the sample were measured from the pattern obtained with an X-ray powder diffractometer (Model Kristalloflex D5000, Siemens, Germany) with a copper tube working at 50 kV and 30 mA. Silicon powder (Reference Material 640b, $a = 5.430940 \text{ \AA}$, National Institute of Standards and Technology, Gaithersburg, MD)¹³ was used as an internal standard by mixing it with dolomite powder. The scanning was made from 20° to $120^\circ 2\theta$ by steps of 0.05° , counting 5 s on every step. The peak positions were measured by fitting with pseudo-Voigt functions and corrected with the internal standard.

(3) Thermal Analysis

Differential thermal analysis (DTA) (STA 409, Netzsch, Germany) was conducted at a heating rate of $2^\circ\text{C}/\text{min}$ from 100 mg isostatically pressed (100 MPa) specimens placed in platinum boats in a flow of dry air.

(4) Neutron Thermodiffraction

Powder neutron diffraction data were collected at the Institute Laue-Langevin (ILL, Grenoble, France) with Instrument D20, a high-flux medium-resolution powder diffractometer equipped with a large-area position-sensitive detector of 1600 cells allowing fast acquisition in a $160^\circ 2\theta$ arc. It operated at a wavelength of 2.4225 \AA .

A furnace was attached to the instrument to provide temperatures up to 1000°C . The heating element, a cylinder made of vanadium, induced a constant-temperature area several centimeters in length along its axis. The temperature was controlled with two chromel–alumel thermocouples located very near the heating element and with an accuracy of $\pm 0.5^\circ\text{C}$.

The dolomite polycrystalline sample was introduced into a silica tube with 0.8 cm internal diameter and 70 cm long; $\sim 5 \text{ g}$ filled the tube up to 6 cm high. The tube was left open to the atmosphere during the heating experiment. Another chromel–alumel thermocouple was introduced inside the powder away from

the neutron beam path, but close enough to be at the same temperature of the region irradiated. By subtracting sample thermocouple readings from those of the furnace control an *in situ* DTA was simultaneously obtained while diffraction data were collected. The beam cross section, 4 cm high and 1 cm wide, assured that the diffracting volume was statistically representative of the sample.

In situ diffraction experiments were carried out by heating the samples from room temperature to 1000°C at a constant heating rate of $2^\circ\text{C}/\text{min}$. Diffraction data as well as temperatures from the thermocouples were recorded continuously. The diffraction patterns were taken sequentially by collecting the neutron counts for 150 s.

(5) Data Analysis

General data processing and plotting were conducted with the help of the commercial package ORIGIN.¹⁴ Rietveld analysis was performed with FULLPROF.¹⁵ The visualization of data in three dimensions with contour projections was made with the help of the commercial package NOESYS.¹⁶ The diffraction data collected during the heating cycle were represented as a sequence of patterns in a pseudo-three-dimensional fashion in which the x -axis corresponds to the diffraction angle 2θ , the y -axis to the temperature, and the z -axis to the relative intensity (Fig. 1(a)). To visualize events such as diffraction line shifts or growth and collapse of phases more precisely, a contour map in two dimensions was also projected from the 3D plot (Fig. 1(b)). The existence of phase domains is clearly highlighted by their diffraction peaks shown in the figure with the corresponding Miller indices.

To follow the process in a more quantitative way some high-intensity diffraction peaks clearly separated from the rest (avoiding overlapping) were selected. Also, the intensities of reflections were individually normalized to one. Therefore, for dolomite, the diffraction intensity of the reflections (006), (104), (102) and a partially overlapping high-order sextet of reflections (204), (108), ($2\bar{1}6$), (116), (009), and (205) were plotted against temperature to monitor its decomposition (Fig. 2). As explained in Section IV, reflection (102) was selected for this purpose since it is the least affected by thermal vibrations.

Reflection (104) was chosen for CaCO_3 and the respective (200) reflections for MgO and CaO . Their variations against temperature are represented in Fig. 3.

III. Results

The room-temperature X-ray diffraction pattern recorded corresponds to a high-purity dolomite with cell parameters $a = 4.8089 \pm 0.0002 \text{ \AA}$ and $c = 16.0154 \pm 0.0006 \text{ \AA}$. The differential thermal analysis of the dolomite exhibited two endotherms with peak temperatures at 760° and at 870°C (Fig. 4).

The evolution *in real time* of the dolomite decomposition can be visualized in the three-dimensional diagram of Fig. 1(a). It is clear from the contour map of Fig. 1(b) that the maximum rate of the dolomite decomposition is in the vicinity of 750°C . Calcium carbonate appears at $\sim 550^\circ\text{C}$ (see diffraction (104), Fig. 1(b)) and decomposes at $\sim 950^\circ\text{C}$ to yield CaO . The generation of MgO from the decomposition of dolomite is also clear. These results are in agreement with the *in situ* DTA plots as can be seen in Fig. 4, where two endotherms are conspicuous at 760° and 960°C .

Another feature clearly shown in Fig. 1(b) is the lattice expansion of the CaCO_3 manifested by the prominent shifts of the reflections (006) and (108).

A more quantitative insight in terms of temperature can be grasped by looking at Fig. 3, where variations of integrated intensities with temperature for selected Bragg reflections are represented. Dolomite commences decomposition at $\sim 500^\circ\text{C}$, while calcite and periclase appear at $\sim 550^\circ\text{C}$.

To obtain the activation energy of dolomite decomposition, the raw integrated intensity of reflection (102) was plotted against temperature. The profile of the decreasing gradient was smoothed

Table I. Chemical Analysis of the Dolomite

Analytical method	Species	Content (wt%)	Theoretical composition (wt%)
Gravimetry	CaO	30.29	30.41
	MgO	22.05	21.83
Ignition loss		47.75	47.73
ICP-plasma	Al_2O_3	0.011	
	SiO_2	0.018	
	Fe_2O_3	0.008	
	TiO_2	0.0014	
	SrO	0.0047	
	MnO	0.0004	
	P_2O_5	0.0059	
	Nb_2O_5	0.0013	
	Flame photometry	Na_2O	0.0018

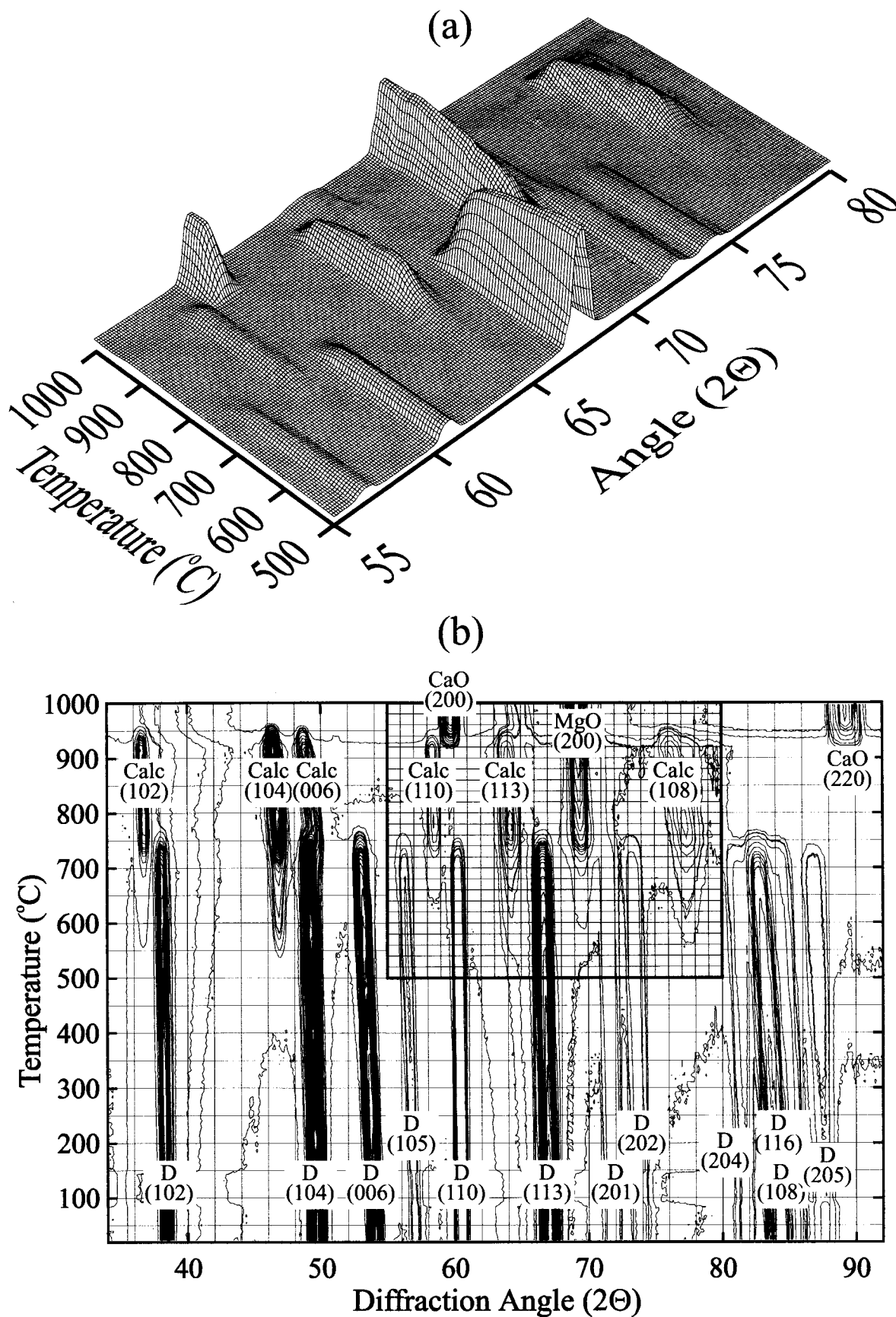


Fig. 1. (a) Sequence of powder neutron diffraction patterns for dolomite as a function of temperature, heating rate 2°C/min, and patterns accumulated for 150 s. (b) Contour map from the three-dimensional elevation of upper sketch: (D) dolomite, (Calc) calcite.

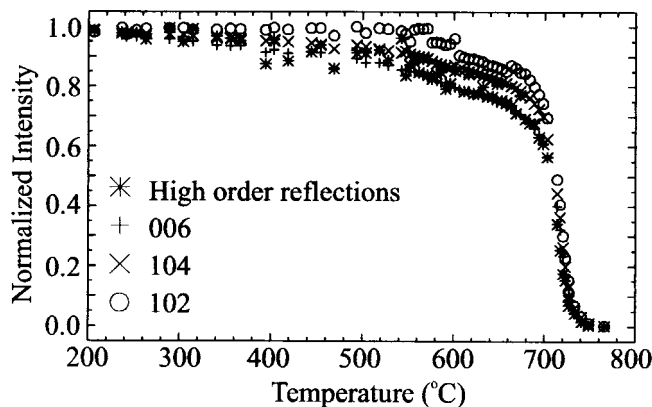


Fig. 2. Integrated intensities versus time for reflections (006), (102) and high-order reflections, which are the sum of (204), (108), (216), (116), (009), and (205), of dolomite during the first loss of CO_2 .

and from it the curve of reaction progress versus temperature was plotted and examined with the expression

$$\ln 3[1 - (1 - \alpha)^{1/3}] - 2 \ln T = \ln AR/E\beta - E/RT \quad (1)$$

derived from the procedure described by Coats and Redfern¹⁷ for nonisothermal experiments and the contracting sphere kinetics model of Hume-Colvin¹⁸ for carbonate decomposition. In the above expression α is the fraction reacted, in the present case 1 minus the normalized intensity of reflection (102), T the absolute temperature in Kelvin, A the frequency factor, R the universal gas constant, E the activation energy, and β the heating rate. To get the activation energy, $\ln 3[1 - (1 - \alpha)^{1/3}] - 2 \ln T$ is represented versus $1/T$ in Fig. 5. The energy obtained for the decomposition process was $47 \text{ kcal}\cdot\text{mol}^{-1}$.

As mentioned previously, the dolomite cell parameters at room temperature were measured by X-ray diffraction (see Section II(2)). The remainder of the values up to 700°C were obtained from neutron diffraction patterns analyzed by the Rietveld method¹⁹ using the analysis program "FULLPROF" developed by J. Rodríguez-Carvajal.¹⁵ The peaks were fitted to pseudo-Voigt functions.

The Rietveld strategy adopted was in accordance with the guidelines of McCusker *et al.*²⁰ The zero shift was fitted using the dolomite cell parameters at room temperature determined by X-ray diffraction. Then this zero shift was a fixed parameter for the refinements with the neutron diffraction patterns at higher temperatures. Asymmetry corrections for the peak were not used, as their shapes were symmetric, at least for the 2θ region explored. To estimate the "goodness of fit" three reliability factors (R_{wp} , R_p and R_B) were calculated¹⁹ and in all cases the obtained values were less than 5%.

The dolomite cell parameters so obtained (a and c) are represented in Fig. 6 and selected data are reported in Table II. The temperature dependence of both parameters from 25° to 700°C was fitted to

$$a = 4.8082 + 1.9277 \times 10^{-5}t + 1.8355 \times 10^{-8}t^2 \quad (2)$$

$$c = 16.066 + 3.3099 \times 10^{-4}t + 1.3653 \times 10^{-7}t^2 \quad (3)$$

where t is the temperature ($^\circ\text{C}$).

It was also possible to conduct Rietveld analysis with the three phase patterns (dolomite, periclase, and calcite) as seen in Fig. 7. The cell parameters a and c for the *in situ* formed calcite are plotted in Fig. 8 with those of Markgraf and Reeder²¹ for a calcite single crystal. The values for the present study, measured in the short temperature interval between 750° and 925°C after dolomite disappearance, are given in Table III.

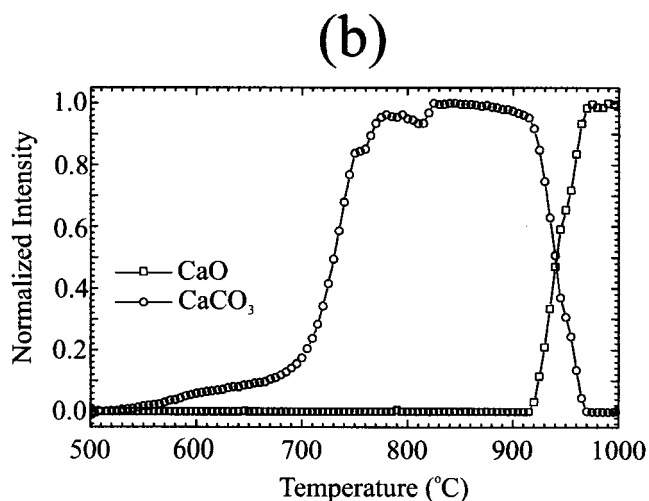
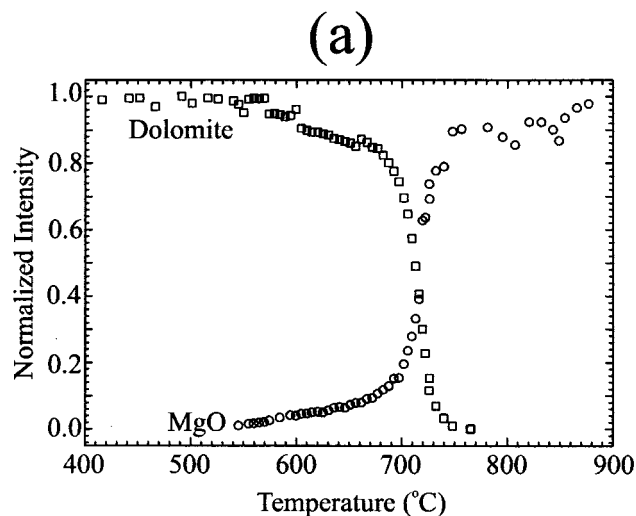


Fig. 3. Reaction progress followed from integrated intensities versus time: (a) reflections (102) of dolomite (\square) and (200) of MgO (\circ); (b) reflections (104) of calcite (\circ) during dolomite decomposition and (200) of CaO (\square) during calcite decomposition.

The relationships between Ca–O and Mg–O bond distances and the temperature can be seen in Fig. 9. All of these data are reported in Table IV.

IV. Discussion of the results

(I) Dolomite Cell Parameters at Room Temperature

From the chemical analysis of dolomite, an almost ideal or stoichiometric formula with a ratio Ca:Mg = 0.987 was determined. Contrary to other dolomite minerals reported in the literature^{7,22} this specimen contains negligible amounts of iron and/or manganese. The room-temperature X-ray parameters $a = 4.8089 \pm 0.0002 \text{ \AA}$ and $c = 16.0154 \pm 0.0006 \text{ \AA}$ differ slightly from the single-crystal values determined by Reeder and Markgraf.²² The dolomite single crystals had a unit cell with $a = 4.8069 \pm 0.0009 \text{ \AA}$ and $c = 16.002 \pm 0.001 \text{ \AA}$. These discrepancies can be attributed to different chemical compositions. The presence of Mn^{2+} or Fe^{2+} in solid solution in the dolomite, with smaller ionic radii²³ than Mg^{2+} , would induce a shrinkage of cell unit. On the other hand, other workers' data from powder²⁴ seem to agree with the present data.

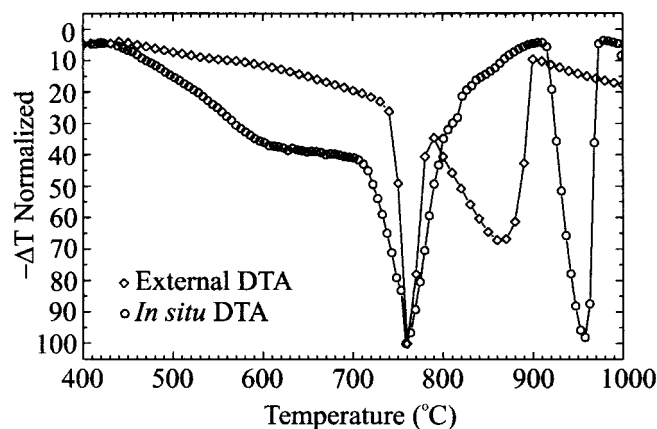


Fig. 4. *In situ* DTA recorded simultaneously with powder diffraction patterns at a heating rate of 2°C/min, depicted with open circles. Conventional DTA of isostatically pressed (100 MPa) dolomite powder, recorded at 2°C/min, highlighted with diamonds.

(2) General Overview of Reactions from 25° to 1000°C

A general sketch of the thermal decomposition of dolomite can be found in Fig. 1(b). It is clear that dolomite decomposes first to yield CaCO₃ and MgO and on further heating calcite breaks up to produce CaO. To get more precision in the temperatures at which these events happen, the integrated intensities of the reflections were plotted against temperature (see Fig. 2). It is worth noting the apparent discrepancy in the decay of integrated intensities. The most likely explanation is that reflections due to planes forming low angles with (001) have an enhanced Debye–Waller factor contribution. Indeed, hexagonal layered structures such as dolomite show a strong thermal anisotropy along the *c*-axis. Consequently, reflections with larger *ℓ* indexes are much more affected by temperature and exhibit a more marked decay. Therefore, to determine the temperature at which the dolomite decomposition starts, it was better to use the (102) reflection, which is the least affected by thermal anisotropy.

Consequently, as can be seen in Fig. 3, a lowering in the profile of the dolomite (102) reflection intensity takes place at ~500°C, indicating the beginning of the dolomite decomposition. Following its decomposition, at ~550°C both MgO and CaCO₃, represented by their reflections (200) and (104), respectively, begin to grow (Fig. 3). Progressing with temperature, 730°C can be considered the point of maximum decomposition rate. From here another interesting observation is evident: MgO and CaCO₃ do not follow

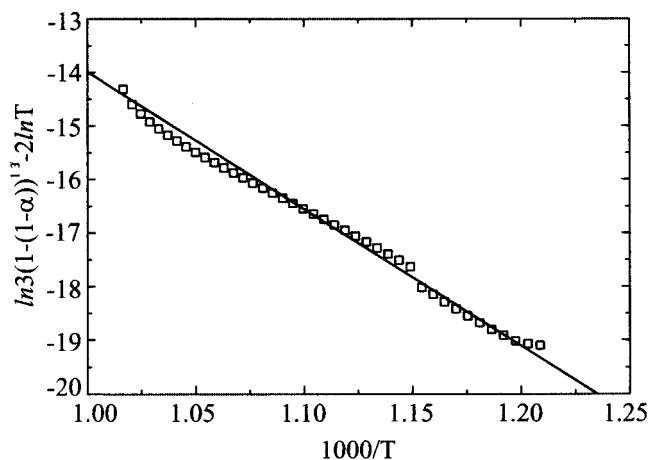


Fig. 5. Plot to obtain activation energy from the slope. Kinetics fitted to contracting sphere model. Squares represent experimental values. Continuous trace represents the fitted straight line.

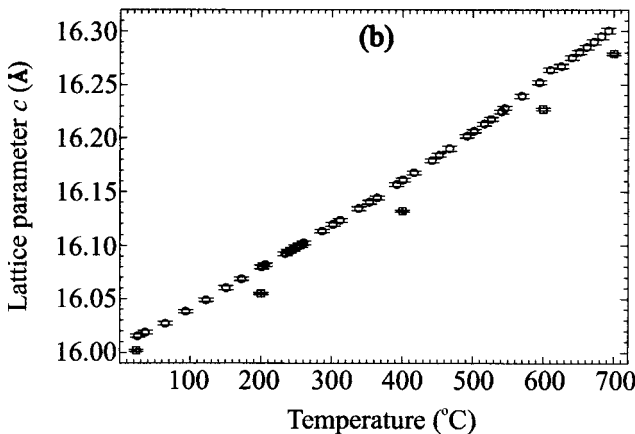
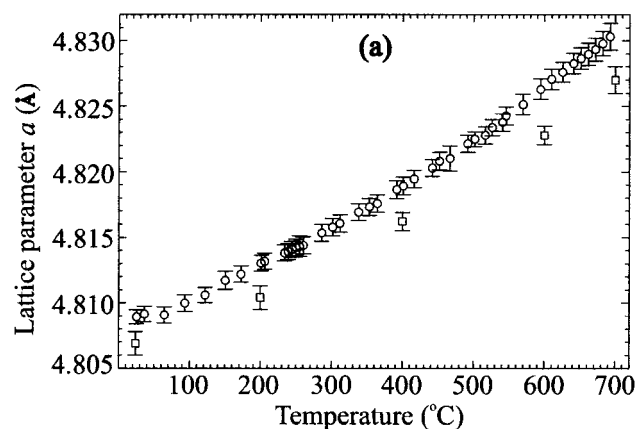


Fig. 6. Unit cell variation of dolomite with temperature, comparing polycrystalline data of present work (open circles) with single-crystal data (open squares) after Reeder and Markgraf.²² Error bars represent standard deviations. (a) Cell parameter *a*; (b) cell parameter *c*.

the same pattern of growth. Calcite grows faster, while MgO is retarded. An explanation for this phenomenon would be consistent with the formation of an intermediate solid solution of formula Ca_{1-x}Mg_x(CO₃) nearer to calcite stoichiometry due to magnesium ions migrating to form MgO. The existence of a magnesium-rich calcite has been reported by Goldsmith and Heard.⁸ These authors found a calcite phase with 20 mol% of magnesium at 900°C. This could also explain the subsequent growth of MgO after calcite decomposition. Indeed, the calcite containing magnesium would

Table II. Cell Parameter Variation with Temperature for the Dolomite Phase[†]

Temperature (°C)	<i>a</i> (Å)	<i>c</i> (Å)	Volume (Å ³)
25.5	4.8089(5)	16.015(1)	320.75(6)
64.6	4.8091(6)	16.027(2)	321.00(6)
93.8	4.8100(6)	16.038(2)	321.35(6)
150.6	4.8117(7)	16.060(2)	322.02(6)
201.1	4.8130(6)	16.080(2)	322.59(6)
250.1	4.8142(6)	16.098(2)	323.12(6)
301.6	4.8158(7)	16.119(2)	323.75(6)
353.2	4.8173(7)	16.140(2)	324.38(6)
401.0	4.8189(7)	16.161(2)	325.01(6)
452.2	4.8208(7)	16.184(2)	325.73(6)
501.6	4.8225(6)	16.207(2)	326.41(6)
545.5	4.8243(7)	16.228(2)	327.08(6)
594.4	4.8263(8)	16.252(2)	327.84(8)
651.3	4.8286(8)	16.280(2)	328.74(8)
692.5	4.830(1)	16.301(3)	329.4(1)

[†]The numbers in parentheses represent the standard deviations for the least significant figures to the left.

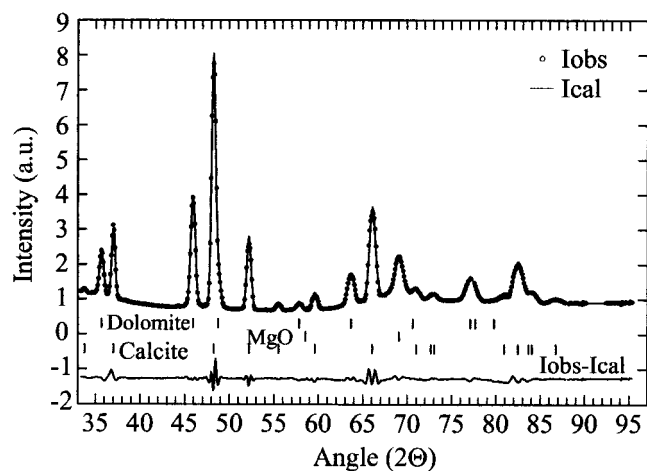


Fig. 7. Neutron diffraction patterns for dolomite sample, treated at 700°C, analyzed by the Rietveld method. Good agreement can be observed between experimental (solid circles) and fitted values (continuous lines) for the pattern combination of the three phases: dolomite, MgO, and calcite.

liberate some Mg^{2+} after its decay, hence increasing the amount of MgO crystals. Other evidence for the formation of a magnesium-rich calcite comes from the lattice parameters measured *in situ*. In particular, the a value is significantly smaller than the one found for pure calcite (see Fig. 8(a)). The presence of a smaller cation

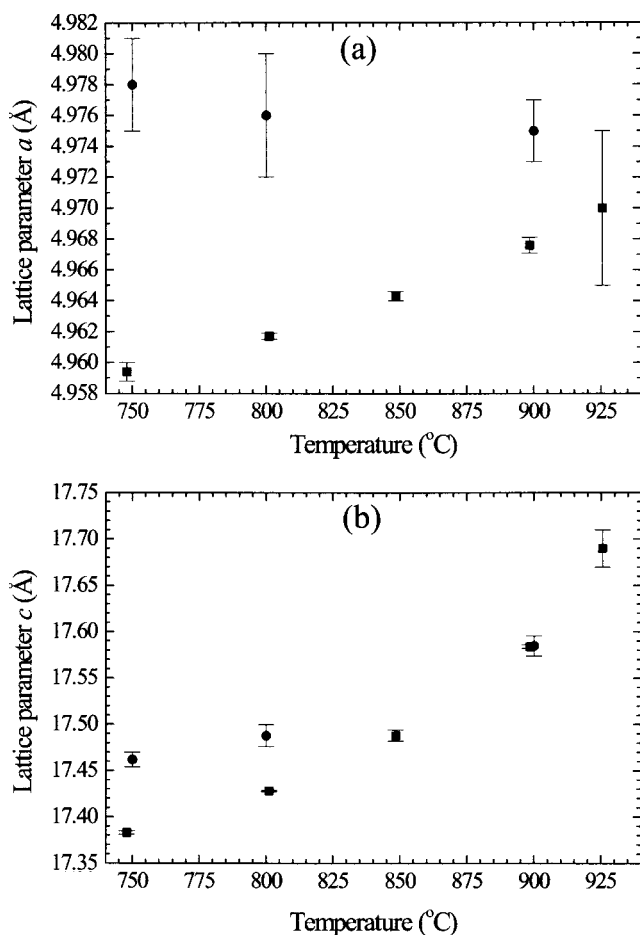


Fig. 8. Variation of unit cell with temperature for *in situ* formed calcite observed in the present work (squares) and for calcite single crystals (circles), after Markgraf and Reeder.²¹ Error bars represent standard deviations. (a) Cell parameter a ; (b) cell parameter c .

Table III. Cell Parameter Variation with Temperature for CaCO_3 [†]

Temperature (°C)	a (Å)	c (Å)	Volume (Å ³)
747.9	4.9594(6)	17.383(2)	370.26(8)
801.1	4.9617(2)	17.4281(6)	371.58(2)
848.4	4.9643(3)	17.487(6)	373.25(4)
894.4	4.9676(5)	17.584(2)	375.80(7)
925.5	4.970(5)	17.69(2)	387.4(6)

[†]The numbers in parentheses represent the standard deviations for the least significant figures to the left.

would shrink the crystal lattice. The magnesium ions are released as the temperature increases. This induces an expansion of the lattice that is manifested by an enlargement of a and c parameters (see Fig. 8).

The above discussion on the breaking up of dolomite is in agreement with the most recent work by Hashimoto *et al.*²⁵ They investigated the decomposition of dolomite into CaCO_3 and MgO under CO_2 atmosphere by isothermal kinetic measurements using X-ray diffraction and electron diffraction techniques. In so doing, they reexamined previous classical theories. As a consequence of their work, they suggested the direct formation of CaCO_3 according to the following mechanism: At the beginning of the decomposition, CO_2 is easily released at defects on the surface of dolomite, leaving O^{2-} . Then, Mg^{2+} ions in the neighboring domains may move to the vicinities of O^{2-} , with Ca^{2+} ions migrating in the opposite direction. The migration or diffusion of these ions occurs in the interfacial zone. CaCO_3 is formed in this zone coherently to the surface of dolomite lattice, mainly by a topotactic process.

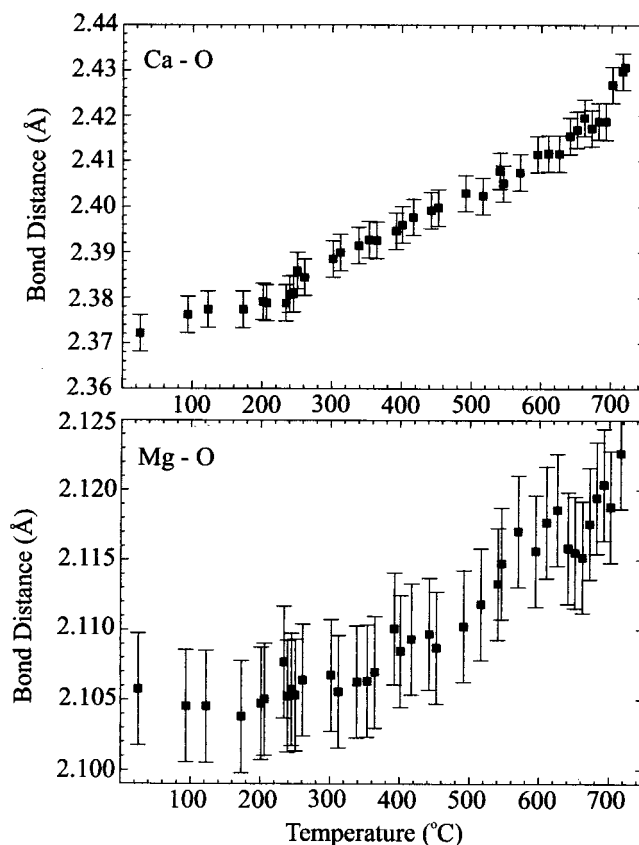


Fig. 9. Changes in distances Ca-O and Mg-O for dolomite with temperature. Values were obtained by Rietveld refinement. Error bars represent standard deviations.

Table IV. Mean Thermal Expansion Coefficients in the Range 25° to 700°C for Cell Parameters and Bond Distances in Dolomite Expressed in 10^{-6} K^{-1}

	α_a	α_c	$\alpha_{\text{Ca-O}}$	$\alpha_{\text{Mg-O}}$
Reeder and Margraf ¹⁹	6.2	25.8	17.6	16.5
Present work	6.7	27.0	35.0 [†]	13.6 [†]

[†]Calculated in the range 200° to 700°C.

(3) Temperatures of Endothermic Effects

The temperature of 730°C, found by diffraction, for the first step, that corresponds to the maximum decomposition rate of dolomite, is in close agreement with the first endothermic peak temperature observed by both conventional and *in situ* DTAs. However, there is an obvious discrepancy in the second endothermic between both DTAs (Fig. 4). Conventional DTA shows the endothermic peak effect at 870°C while the *in situ* DTA shows the same effect at ~965°C in accordance with the thermodiffraction data (Fig. 3). The root of this apparent disagreement is the strong dependence of the CaCO_3 decomposition on the CO_2 partial pressure. The higher the CO_2 partial pressure, the more difficult it will be for the reaction to progress. This is translated into a higher temperature to complete the decomposition. Furthermore, the conventional DTA was obtained under a low partial pressure of CO_2 , not greater than the CO_2 partial pressure of the ambient atmosphere. However, the *in situ* DTA was performed on a larger sample, ~5 g, and although the tube was open to the external atmosphere, most of the CO_2 released in the first step was likely to remain in the tube because there was no stream of air, and CO_2 is denser than air. Therefore, although not measured, a nonnegligible CO_2 partial pressure was built up at the bottom of the tube, with the described consequences.

(4) Kinetics of Dolomite Decarbonation

There are no data reported in the literature on the kinetics of dolomite decomposition by TGA or DTA under nonisothermal conditions. The only data available on the decomposition of dolomite, in the range 477° to 517°C, are in the study of Powell and Searcy²⁶ by the torsion-effusion and torsion-Langmuir techniques. From their data it was concluded that the activation enthalpy is $46.5 \text{ kcal}\cdot\text{mol}^{-1}$ for decomposition. Unfortunately, TGA and DTA experiments cannot be used to calculate dolomite decomposition activation energy because these techniques do not allow a clear separation of the two endotherms. An alternative method is therefore neutron thermodiffraction since the decarbonation is clear and neat through the decay of diffraction intensities. Then, as mentioned previously, the energy obtained for the decomposition of dolomite was $47 \text{ kcal}\cdot\text{mol}^{-1}$. This is in agreement with the value obtained by Powell and Searcy for dolomite decomposition and is in line with those published by Carrizosa *et al.*¹⁸ in their study of CaCO_3 decomposition, and by Kissinger²⁷ studying magnesite and calcite.

(5) Thermal Expansion of Dolomite and Calcite

Other relevant information emerging from these thermodiffraction experiments is the cell parameter variation of the crystalline phases involved. Dolomite cell parameters vary according to parabolic laws (Eqs. (2) and (3)). Because of different chemical composition, as explained in Section II, a systematic shift toward higher values with respect to single-crystal data²² is quite apparent (see Fig. 6 and Table II).

Thermal expansion coefficients were calculated from the cell parameter variation with temperature. Thus, the dolomite mean thermal expansion coefficient between 25° and 700°C obtained along the *a*-axis is $(6.7 \pm 0.4) \times 10^{-6} \text{ K}^{-1}$ and that along the *c*-axis is $(27.0 \pm 0.2) \times 10^{-6} \text{ K}^{-1}$.

These values agree with those obtained by Reeder and Markgraf,²³ within the statistical limits of confidence. The anisotropy is apparent, as expected for a hexagonal-type crystal structure, although not as extreme as in other minerals.

On the other hand, cell parameter variations between 748° and 925°C calculated for calcite (Table III) do not agree with those reported by Markgraf and Reeder²¹ for calcium carbonate between 24° and 900°C. The most remarkable feature of the Markgraf and Reeder data is the shrinkage of the cell parameter *a* from 4.978 to 4.977 Å. Nevertheless, the decreasing trend is not so obvious in the region above 750°C because the statistic confidence bars are larger than the thermal variations. On the other hand, the *c* parameter variation is clearer and increases from 17.46 to 17.58 Å.

The present calcite values are significantly higher than the ones of Markgraf and Reeder,²¹ but these discrepancies are only apparent. It has to be taken into account that the neutron diffraction results have been obtained under quite different conditions; the calcite is the result of dolomite decomposition and is immersed in complex solid-state reaction equilibrium. On the other hand, the data of Markgraf and Reeder²¹ were obtained from a single crystal specimen.

Indeed, the calcite cell parameters calculated in the present work probably highlight that the calcite formed contains some Mg^{2+} and is crystallizing over a *host* dolomite structure which strongly influences crystal growth of calcite. These last inferences would support the diffusion mechanism as explained before.

(6) Bond Thermal Expansion in Dolomite

The precision compared with single-crystal studies is lower but a trend in bond distances clearly emerges. The variations for Ca–O and Mg–O can be seen in Fig. 9. It seems that after ~200°C there is a definite expansion. That is why least-squares fitting was applied between 200° and 700°C. From the slope, mean thermal expansion parameters were estimated. For Mg–O the value found in this work ($13.6 \times 10^{-6} \text{ K}^{-1}$) is comparable with the one previously published ($16.5 \times 10^{-6} \text{ K}^{-1}$).²³ However, there is an obvious discrepancy for Ca–O; in this work a value of $35 \times 10^{-6} \text{ K}^{-1}$ was found compared with $17.6 \times 10^{-6} \text{ K}^{-1}$ reported by Reeder and Markgraf.²³

V. Conclusions

Neutron diffraction time-resolved experiments were conducted for dolomite for the first time. It has been shown that the decomposition of dolomite in air takes place in two stages. Calcium carbonate is released with magnesium oxide initially and, on further heating, calcium carbonate collapses to yield calcium oxide. It has been verified too, from changes in diffraction intensities, that dolomite starts to break up around 500°C with the maximum decomposition rate being observed at 730°C.

The cell parameters of dolomite have been measured from 25° to 700°C. The variation, although continuous, is not truly linear. As expected, the expansion along the *c* direction is larger than along the *a* direction. The mean linear thermal expansion agrees with previous studies published for single-crystal specimens.

The short life of calcium carbonate after dolomite disappearance has been explored measuring its cell parameters at temperatures ranging from 748° to 925°C.

The curves expressing the evolution of diffraction intensities as a function of temperature are well-defined, having good statistics, and very small noise. This indicates that neutron thermodiffraction under nonisothermal conditions is suitable for studying high-temperature decomposition kinetics.

Acknowledgments

We thank Dr. A. Hidalgo for valuable help and assistance during the neutron experiments. We also thank to Prodomasa for kindly providing specimens from their quarries in Coín (Spain). Beam time was granted by ILL, Exp. No. 5-25-25.

References

1. A. Skillen, "Limestone and Dolomite: The Ubiquitous Fluxes in Raw Materials for the Glass and Ceramics Industries," *Ind. Miner.*, 44–49 (1993).

- ²A. H. de Aza, P. Pena, R. Torrecillas, and S. de Aza, "New Spinel Containing Calcium Aluminate Cements," *Br. Ceram. Proc.*, **60** [1] 261–62 (1999).
- ³A. H. de Aza, "Design and Development of High Alumina Materials with Spinel and Calcium Hexaluminate in the Matrixes" (in Spanish); Ph.D. Thesis. Universidad Autónoma de Madrid, Madrid, Spain, 1997.
- ⁴J. L. Rodríguez, M. A. Rodríguez, S. de Aza, and P. Pena, "Reaction Sintering of Zircon–Dolomite Mixtures," *J. Eur. Ceram. Soc.*, **21** [3] 343–54 (2001).
- ⁵A. H. de Aza, P. Pena, and J. S. Moya, "Reactive Coating of Dolomite on Alumina Substrates," *J. Eur. Ceram. Soc.*, **17**, 935–41 (1997).
- ⁶R. W. G. Wyckoff, *Crystal Structures*, Vol. 2, 2nd Ed.; pp. 466–68. Interscience, New York, 1967.
- ⁷L. Y. Chang, R. A. Howie, and J. Zussman, "Dolomite"; pp. 189–218 in *Rock-Forming Minerals*, Vol. 5B, *Non-Silicates: Sulphates, Carbonates, Phosphates, Halides*. Longman Group Ltd., London, U.K., 1996.
- ⁸J. R. Goldsmith and H. C. Heard, "Subsolidus Phase Relations in the System $\text{CaCO}_3\text{--MgCO}_3$," *J. Geol.*, **69**, 45–74 (1961).
- ⁹R. A. W. Haul and H. Heysyk, "Differential Thermal Analysis of the Dolomite Decomposition," *Am. Mineral.*, **37**, 166–79 (1952).
- ¹⁰R. Otsuka, "Recent Studies on the Decomposition of the Dolomite Group by Thermal Analysis," *Thermochim. Acta*, **100**, 69–80 (1986).
- ¹¹I. Martínez, J. Zhang, and R. J. Reeder, "In Situ X-ray Diffraction Aragonite and Dolomite at High-Pressure," *Am. Mineral.*, **81**, 611–24 (1996).
- ¹²P. Engler, M. W. Santana, M. L. Mittleman, and D. Balazs, "High Temperature X-ray Diffraction Techniques for Enhancing Time/Temperature Resolution," *Thermochim. Acta*, **130**, 309–18 (1988).
- ¹³C. R. Hubbard, H. E. Swanson, and F. A. Mauer, "A Silicon Powder Diffraction Standard Reference Material," *J. Appl. Crystallogr.*, **8**, 45 (1975).
- ¹⁴Program ORIGIN, Version 5.0, Microcal Software Inc., Northampton, MA.
- ¹⁵J. Rodríguez Carvajal, Program FULLPROF, Version 3.5d, 1998.
- ¹⁶Program NOESYS, Version 1.2, Fortner Software LLC, Sterling, VA.
- ¹⁷A. W. Coats and J. P. Redfern, "Kinetic Parameters from Thermogravimetric Data," *Nature (London)*, **201** [1] 68–69 (1964).
- ¹⁸I. Carrizosa, J. M. Criado, F. Gonzalez Garcia, and M. Gonzalez, "Influencia de las Condiciones Experimentales en la Cinética de las Reacción de Descomposición Térmica de CaCO_3 ," *Bol. Soc. Esp. Cerám. Vidrio*, **17** [1] 23–27 (1978).
- ¹⁹F. Izumi; Ch. 13 in *The Rietveld Method*. Edited by R. A. Young. Oxford University Press, Oxford, U.K. 1993.
- ²⁰L. B. McCusker, R. B. Von Dreele, D. E. Cox, D. Louer, and P. Scardi, "Rietveld Refinement Guidelines," *J. Appl. Crystallogr.*, **32**, 36–50 (1999).
- ²¹S. A. Markgraf and R. J. Reeder, "High Temperature Structure Refinements of Calcite and Magnesite," *Am. Mineral.*, **70**, 590–600 (1985).
- ²²R. J. Reeder and S. A. Markgraf, "High Temperature Crystal Chemistry of Dolomite," *Am. Mineral.*, **71**, 795–804 (1986).
- ²³R. D. Shannon and C. T. Prewitt, "Effective Ionic Radii on Oxides and Fluorides," *Acta Crystallogr.*, **B25**, 925–45 (1969).
- ²⁴L. Keller and G. S. McCarthy, PDF 36-426 for $\text{CaMg}(\text{CO}_3)_2$. International Centre for Diffraction Data, Newton Square, PA.
- ²⁵H. Hashimoto, E. Komaki, F. Hayashi, and U. Uematsu, "Partial Decomposition of Dolomite in CO_2 ," *J. Solid State Chem.*, **33**, 181–88 (1980).
- ²⁶E. K. Powell and A. W. Searcy, "Kinetics and Thermodynamics of the Composition of Dolomite and Metastable Solid Product," *J. Am. Ceram. Soc.*, **61** [3] 216–21 (1978).
- ²⁷H. E. Kissinger, "Reaction Kinetics in Differential Thermal Analysis," *Anal. Chem.*, **29** [11] 1702–706 (1957). □